Comparison of Titan's Equatorial Dunes to Lambertian Titan Surface Simulations*

Gabriel M Steward,[1] Jason W. Barnes,[1] William Miller,[1] and Shannon MacKenzie[2]

[1]*University of Idaho, Moscow, Idaho 83844*

[2]*Johns Hopkins University Applied Physics Laboratory, Laurel, Maryland 20723*

ABSTRACT

NOTE: Red notes are important! Do not submit the document with any of them remaining!

NOTE: Blue notes are placeholders! Do not submit the document with any of them remaining!

The nature of Titan's surface is poorly understood, largely due to the atmosphere's extensive interference. To handle this interference, we simulate Lambertian Titan models using the radiative transfer program SRTC++ at different surface albedos. We then compare these models to real data from Cassini VIMS (Visual and Infrared Mapping Spectrometer) of the Huygens landing site and equatorial dunes. We confirm that SRTC++ produces reasonable simulations for Lambertian surfaces shrouded by Titan's atmosphere in many, but not all, situations. Furthermore, we find that Titan's dunes act as Lambertian surfaces, with all identified deviations correlating to suspected SRTC++ or atmospheric model deficiencies. We also perform a targeted search for an opposition effect on Titan's dunes through VIMS observations and find none, though the effect could conceivably be too narrow to observe.

Keywords: KEYWORDS (111) — KEYWORDS (112)

1. INTRODUCTION

Titan has one of the least understood surfaces in the entire Solar System, due largely to its thick haze-filled atmosphere that is opaque to most light. While there do exist a handful of atmospheric "windows" through which specific wavelengths of light can pass through relatively unimpeded (Barnes et al. 2007), only limited spectral information on the surface can be gleaned through them. Even within the windows, the thick atmosphere contaminates the relatively small amount of surface information we do receive; transmission is a combination of surface and atmospheric effects (Es-sayeh et al. 2023).

To combat the atmospheric contamination, we turn to radiative transfer models of Titan's atmosphere that compute the influence the atmosphere has on the received signal, allowing for true surface effects to be identified. Many such models have been created over the years, each with their own strengths and weaknesses (Vinatier et al. (2007); Griffith et al. (2012); Xu et al. (2013); Barnes et al. (2018); Rodriguez et al. (2018); Corlies et al. (2021); Rannou et al. (2021); and Es-sayeh et al. (2023), to name a few). These radiative transfer models depend on accurate knowledge of Titan's atmosphere, which is most well characterized at the moon's equatorial regions since that is where the Huygens lander mea-

sured the atmosphere in situ (Tomasko et al. 2008). Many surface characterization studies attempting to filter out the influence of the atmosphere have been performed in the past (Buratti et al. 2006; Soderblom et al. 2009; Kazeminejad et al. 2011; Brossier et al. 2018; Es-sayeh et al. 2023; Solomonidou et al. 2024). However, the majority of them make a notable assumption: that the surface behaves as a Lambertian reflector; a perfect scatterer with no directly reflected components. Buratti et al. (2006) is a notable exception.

Few, if any, surfaces in the Solar System are truly Lambertian due to the prevalent opposition effect (Déau et al. 2009; Schröder & Keller 2009). We might expect for Titan's surface to exhibit similar non-Lambertian behaviors, but first-order analysis of the moon as a whole in the IR (infrared) shows a Lambertian surface (Le Mouélic et al. 2019, 2012). On the other hand, the one observation we have from the ground on Titan, the Huygens lander, did report an opposition effect (Schröder & Keller 2009; Karkoschka et al. 2012). However, Huygens landed in a "dark blue" region (Rodriguez et al. 2006), which is an uncommon terrain on Titan's surface (Keller et al. 2008). For Titan as a whole, Radar observations that show an opposition effect (Neish et al. 2010; Wye 2011), but given the drastically different length scales probed between radar (centimeters) and IR (microns), we have no reason to believe they would be similar.

Our primary science goal within this paper is to better understand Titan's surface properties by creating Lambertian Titan radiative transfer simulations and comparing them to real observations of the dunes. Our goal is primarily accomplished through determining whether, or to what extent, Titan's dunes are Lambertian in reflected IR sunlight. In the process of the Lambertian alaysis, we attain information about the dunes' abledo in various IR wavelengths and identify differing behaviors between said wavelengths.

The vast majority of observations of Titan's surface have been done by spacecraft visiting Saturn, with the most high-quality data coming from the Cassini mission. As such, many images of Titan's surface are taken at unusual viewing geometries. Such observations are quite useful, as it allows characterization of Titan's surface from a wide variety of orientations, making it easier to determine how non-Lambertian a terrain is. Unfortunately, most current radiative transfer models applicable to Titan either assume a plane parallel atmosphere in their calculations (Griffith et al. 2012; Es-sayeh et al. 2023), don't consider angle at all (Rannou et al. 2021), or use a spherical approximation (Corlies et al. 2021). Thus, all these radiative transfer models lose accuracy the further the viewing geometry is from direct illumination, and would miss potential non-Lambertian effects.

To gain the useful information contained within observations at non-ideal viewing geometries, the spherical nature of Titan's atmosphere must be considered. Thus, we create forward modeled simulations of a Lambertian Titan using SRTC++ (Spherical Radiative Transfer in C++), a radiative transfer code tailored to model Titan in full spherical geometry at the infrared wavelengths available to Cassini's VIMS (Visual and Infrared Mapping Spectrometer) instrument (Barnes et al. 2018). Other spherical models do exist (Xu et al. 2013), but we chose SRTC++ due to familiarity with the code.

Once we were equipped with a spherical radiative transfer model and atmospheric characterization from Huygens, we could compare simulations with reality on a scale covering the entire Cassini mission. As the equatorial regions are the best characterized atmospherically, we chose to examine the terrain there. While we examined multiple terrain types, it was determined that only the equatorial dunes had a sufficient number of reliable observations from which meaningful conclusions could be drawn. We also hand-picked observations from the Huygens landing site for the sake of comparison, even though that location was only viewed at a limited number of viewing angles. For both the dunes and the Huygens landing site we compiled VIMS observations from across the entire Cassini mission over all available viewing geometries, limiting observations to only those judged to be of sufficient quality.

This analysis serves dual purposes–to better understand Titan's surface properties, and to qualitatively validate the SRTC++ simulation against real data. To accomplish these goals, first we outline improvements made to SRTC++ in Section 2 and report on those the results of those changes in Section 3. We describe the procedure by which we gathered our Titan data in Section 4, compare reality to simulation in Section 5 for both the Huygens landing site and dunes, and perform a specific search for the opposition effect in Section 6. Lastly, we conclude in Section 7.

2. RADIATIVE TRANSFER MODEL METHODS
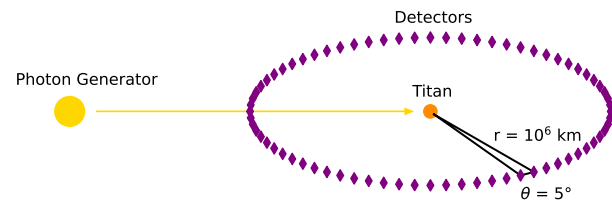
METHODS: Jason's Section. Brief summary of SRTC++, citing the previous paper for more details. Describe new SRTC++ modules used, notably Absorption and the switch to Doose atmosphere. There should be a comparison figure to note the differences between the two. Mention the new integration method.

Figs: comparison between SRTC++ versions.

Will be done by Jason

For our work, we used SRTC++ to create three different simulations of a uniformly Lambertian Titan, each run with a different surface albedo: 0.0, 0.1, and 0.2. Besides the albedo, the simulations were set up with identical parameters, as shown in Figure 1. The virtual detectors were set 10,000 km away from the Lambertian Titan, separated by 5 degrees and completely encircling the moon. Output was generated at all eight VIMS IR wavelength windows for Titan's atmosphere: 0.93, 1.08, 1.27, 1.59, 2.01, 2.69, 2.79, and 5.00 μm.
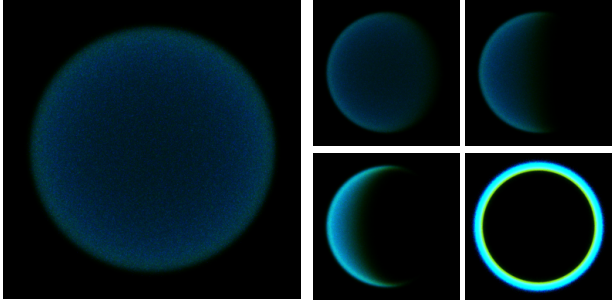
3. SIMULATION RESULTS
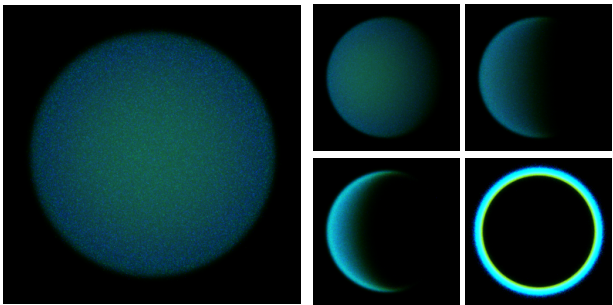
Figure 1. Layout of our SRTC++ simulations. Distances not to scale. Detectors are all equidistant from Titan and angular separation is the same for each one. The yellow arrow represents "photon packets" being shot at Titan. The "photon packets" do not interact with the detector they initially pass through on their way to Titan.

Figures 2 and 3 show the results of the simulations at 0.0 and 0.1 albedo, respectively, colored with 5.00 μm as red, 2.01 μm as green, and 1.27 μm as blue, as done in Barnes et al. (2005). The results of 0.1 albedo are closest to the

"greenish" pictures of Titan in Barnes et al. (2005), though naturally without any terrain variation. Not shown is a simulation run at 0.2 albedo, which is similar to the 0.1 result, but a brighter green.


Figure 2. Simulation results for a Lambertian Titan with 0.0 albedo, colored with 5, 2, and 1.3 μm mapped to red, green, and blue, respectively. Left image is viewed at 0° from the incidence angle. Right four images are, clockwise from the top left, at 35°, 90°, 180°, and 120°, respectively. **Animating Version: A0.0LambertSimMOVIE.gif**

Figure 3. Same as Figure 2 but for 0.1 Albedo. **Animating Version: A0.1LambertSimMOVIE.gif**

The simulations are largely as expected for a Lambertian sphere obscured by a thick atmosphere. Pont & Koenderink (2007) shows what a Lambertian sphere should be without an atmosphere from Figure 9, and the 0.0 albedo simulation shows us the effect of the atmosphere without any signal coming from the surface. Both atmospheric and surface effects should be active in the 0.1 and 0.2 albedo simulations, and that is what we see in the directly illuminated view: a greenish center where there's minimal atmospheric influence that slowly fades off as the emission angle becomes steeper, at which point the atmosphere takes over with its bluish hue. Note that the coloration is entirely due to atmospheric effects; bluer light is scattered by atmospheric haze more readily than redder light. In the raw data, the blue channel is the largest even in the center at 0.1 albedo. It is merely the choice of color balancing that gives Titan its greenish hue; a sensible choice as it allows us to readily identify places with more

surface signal than atmospheric. The center of the disc, when viewed from head-on, is rather uniform with little variation, as expected.

Views other than at zero phase also behave as expected; the limb is atmospherically dominated, becoming bluer. Light is more likely to be forward scattered than backscattered in Titan's atmosphere (García Muñoz et al. 2017; Cooper et al. 2025), so the closer the Sun gets to behind Titan, the brighter the limb becomes. A Lambertian surface without an atmosphere would have no light coming from anywhere that was not directly illuminated, but we see a small amount of light from beyond the terminator due to atmospheric scattering. We can also see the shadow Titan casts on its own atmosphere in the profile views as the signal gets abruptly diminished near the top and bottom of the moon, but the atmosphere above this shadow remains illuminated. This effect is known to happen on Earth as well and is what causes the colors of twilight (Lynch & Livingston 2004).

Notably, the "eclipse" view at 180 degrees is functionally identical in all simulations, which it should be as the surface has little influence on the signal at this viewing geometry. There is most certainly interesting science to be done with the simulation at this angle to probe the atmosphere, but such investigations are beyond the scope of this paper.

The simulation results notably appear slightly grainy, due to the Monte-Carlo nature of SRTC++. If we were to run the simulation for longer, the S/N (signal to noise ratio) would increase, and the overall image result would become smoother. Instead, we average numerous spectels together in each histogram bin to increase the S/N for combined spectels.
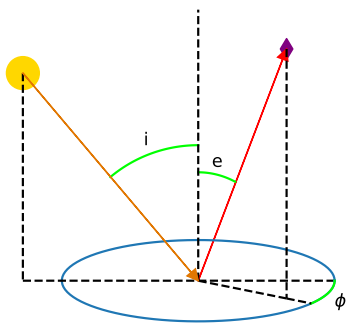
We ultimately seek to compare these simulations with real data. And while we can qualitatively see that real Titan images do have similar coloration and limb effects (Barnes et al. 2005), the fact that real Titan has numerous different terrain types interferes with any more robust conclusions. Thus, we transformed the simulations to present their data based on viewing gometry information, rather than producing visual information. The transformed simulations can, given a specific viewing geometry, describe how a Lambertian Titan would appear at that geometry, which can then be compared to real data. These simulations were effectively transformed into numerical bidirectional reflectance distribution functions (BRDFs).

To construct these transformed simulations, every spectel was sorted into bins based on viewing geometry, and then their values were averaged. The bins were separated by 5° increments in incidence, emission, and azimuth angle, defined as shown in Figure 4, with 0° azimuth being the forward scattering direction, and 180° being backscattering.

Notably, our transformed simulations have only three angles, while more traditional BRDFs have four. We do not treat topographic changes in a surface, as such information

is very context dependent, so we can safely assume that the sun as always coming in from the same direction, removing the need to keep track of the fourth viewing angle. As such, we will call these transformed simulations restricted BRDFs from here on out. This choice also makes it easier to determine when backscattering or forward scattering is occurring, key indicators of non-Lambertian behavior.

Viewing Geometry Model: Incidence 40 Emission 23 Azimuth 34

Figure 4. Viewing geometry angles used in this paper. Incidence angle is represented by "i", emission angle by "e", and azimuth angle by "ϕ". The arrows trace out a path from the sun (yellow circle), to some arbitrary spot on Titan's surface, to a detector (purple diamond). Diagrams modeled after this one appear in future figures to give context for the data.

With 3 different albedos and 8 wavelengths, we produced a total of 24 restricted BRDFs ready to be compared with other restricted BRDFs compiled from real VIMS data.

4. OBSERVATIONS AND DATA

Cassini performed 127 close flybys of Titan during its mission (Seal & Bittner 2017), and most of those flybys have observations from Cassini VIMS. Viewing geometries on any single flyby are generally limited in scope, as the spacecraft itself could only examine geometries it personally encountered. Thus, in order to gain a proper understanding of the surface of Titan at a wide range of viewing geometries, we used observations from as many flybys as possible.

The primary obstacle in properly using all the data is the sheer quantity; 127 flybys, tens of thousands of individual observations, and in each of those hundreds of pixels, with 256 spectels each. If we wished to make a single global model, this would not be an issue, as an algorithm could easily ingest everything. However, simple inspection of VIMS images reveals that different terrains have different albedos, and our simulations in Figures 2 and 3 clearly show how much the appearance of the surface changes with albedo. Averaging all terrain types together could smooth out non-

Lambertian behavior, or allow a single non-Lambertian terrain type to contaminate all the others.

As such, we focus our analysis based on terrain types. We primarily investigate the equatorial regions between 30° and -30° latitude since that's where Huygens sampled the atmosphere (Tomasko et al. 2008), making this region the best characterized. We also want terrain types that are viewed from a wide variety of viewing geometries with a large number of reliable observations. We judged that only Titan's dunes met all these criteria. (The equatorial bright terrain was considered as well, but the results we obtained from it were inconsistent and unreliable.) In pursuit of this goal, we created a raster mask of Titan's equatorial dunes in Figure 5. The resolution in question for the mask is one pixel per degree on Titan's surface; 181 in latitude and 360 in longitude.
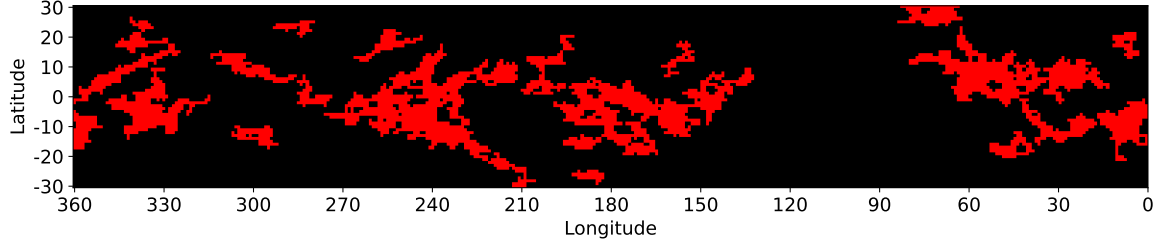
The creation of the mask began with the Titan terrain map created by Lopes et al. (2020) using radar data. VIMS observations, which are taken in infrared, often don't match the radar observations (Soderblom et al. 2007), but tend to agree in the bulk of major features; most notably (and importantly for this paper), the dunes have good agreement on a global scale.

VIMS observations come in the form of files called cubes. Our investigation procedure for these files began with a basic database search; in our specific case, we looked for any cubes that had pixels in the equatorial regions between 30 and -30 latitude, and also had pixels of 25 km ground resolution or finer. The database we were using had already filtered out clearly erroneous files, as well as so-called "noodle" images which are only a handful of pixels in diameter. The cubes themselves were calibrated with the standard VIMS pipeline (Barnes et al. 2007).

We then binned spectels within each pixel in the list and created a restricted BRDF out of them in a process identical to that described in Section 3. Unlike other investigations, we did not subtract off atmospheric contributions, as our simulations include atmospheric contributions. Retaining atmospheric contributions saved us considerable processing difficulties.

There are a few limitations to the created restricted BRDFs. The primary limitation is that certain viewing angles, usually at the extreme ends of allowed values, do not exist since Cassini was never in those positions. There was also no check for interfering clouds during the creation process.

Particularly fine-resolution cubes can separate spectral end members that are mixed together in coarser observations and thus are not reflected in the mask, such as a handful of observations that can see interdune areas (Barnes et al. 2008). These pure spectral endmembers need not match the behavior of the terrain they are surrounded by, and could conceivably offset the final model. The interdune areas are known to vary considerably across Titan (Bonnefoy et al. 2016).

Figure 5. Titan equatorial surface terrain mask for dunes, as informed by Lopes et al. (2020) mixed with VIMS observations. The red pixels are dunes, black is everything else. Almost all of the dunes on Titan are included in this mask, though there are a few regions outside the 30° and -30° latitude boundaries.

Fortunately, the restricted BRDF created for the dunes exhibited remarkable consistency and order, despite the interdunes' presence. We are unsure precisely why this is–it could be that a single kind of interdune dominates most of Titan's dunes, and all others are insignificant, making the result orderly. Alternatively, the various interdune types could simply be drowned out by the sheer amount of data averaging occurring. This relatively smooth result is somewhat remarkable as the equatorial bright terrain's restricted BRDF was decidedly disorderly, despite it not having a known equivalent of interdune interference.

Any retrieved albedos from this model will most likely be biased higher than pure dune sands, given the brighter interdunes (Bonnefoy et al. 2016). However, as we are examining the dunes terrain type as a whole, we do not consider this as a detriment to any of our results.

In addition to the dunes, we also derived a restricted BRDF for the Huygens landing site, to allow for comparison to observations made by the Huygens lander (Tomasko et al. 2008). We performed a database search similarly to how we made the other models, but we also went in manually rather than using a mask, cleaning up any situations where the wrong latitude and longitude were obtained due to ephemeris uncertainties most likely sourced from within the program SPICE (**?**) used to retrieve metadata. This ensured that the data were devoid of any contamination; a caution we only had to exercise since the Huygens landing site was such a small area on the boundary of multiple terrain types.

In order to counteract the lack of observational geometries for both the dunes and the Huygens landing site, we performed tetrahedral interpolation to fill in as many observation angles as possible in the restricted BRDFs using the PyVista package (Sullivan & Kaszynski 2019).

5. SIMULATION VS DATA COMPARISON

5.1. *Huygens Landing Site*

We choose to examine the Huygens landing site first as its data set is simpler, covering significantly fewer viewing geometries than the dunes. As three-dimensional data (i,e, and ϕ in this case) are hard to visualize, we opt to plot individual one-dimensional "skewers" of data at a time, fixing two of the three viewing geometry angles while allowing the third to vary. We create skewers for all restricted BRDFs, be they simulations or real data. We plot select representative skewers of the three simulations and Huygens landing site data in Figures 6-8.
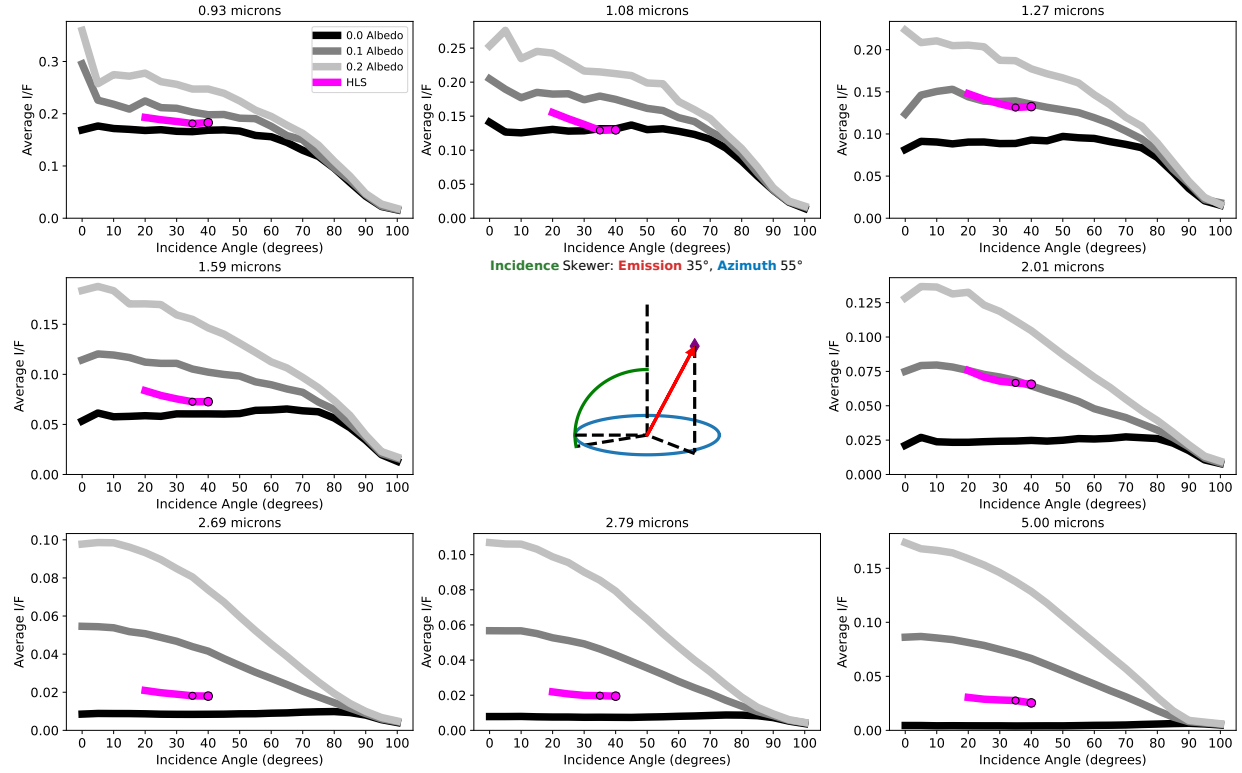
The simulated numerical restricted BRDFs showcase a distinct shifting of behavior across the various wavelengths. Shorter wavelengths show higher I/F **(?expandronym?)** as light traverses through a higher optical depth of highly reflective haze aerosols (Es-sayeh et al. 2023), allowing for more scattering events in more directions.

We see characteristic behavioral differences in restricted BRDF behavior at the different wavelengths in Figure 6 and Figure 7, with the general shape of emission skewers in particular changing drastically between 0.93 and 5.00 μm. When skewering across incidence or emission, such variability is common; though when skewering across azimuth, the general shape is usually similar in all wavelengths, including the skewer shown in Figure 8. Keep in mind that across these three figures, only a small selection of the total three-dimensional histogram is shown; behavior can change significantly when skewering at different i, e, or ϕ values, though the transitions are always relatively smooth. These particular skewers were chosen because they have the best Huygens landing site data visualizations.

The Huygens landing site data are very well behaved for the most part, interpolating smoothly and forming lines that correspond rather well to the simulations. In 1.27 and 2.01 μm, the data line up almost perfectly with the 0.1 albedo simulation, while the others sit parallell between 0.0 and 0.1 albedo. 1.08 μm hugs the 0.0 albedo line, and of all the wavelengths, it shows the largest deviation from parallell to the simulation, most notable in Figure 6. We are unsure why 1.08 μm in particular deviates from the simulated curve because we expect 0.93 and 1.08 μm data to deviate similarly due to the large atmospheric contributions and unmodeled Rayleigh scattering at these shorter wavelengths.

Even considering 1.08 μm's quirks, the Huygens landing site appears consistent with a Lambertian surface in the limited viewing geometries to which we have access, which admittedly is not very many. We chose the best skewers we

Figure 6. Incidence angle skewer for the Huygens landing site: here we plot average I/F versus incidence angle comparing restricted BDRF with Huygens landing site data with fixed emission and azimuth angles. All eight wavelengths are arranged from shortest to longest, with the central area occupied by a geometry diagram to illustrate the specific geometry bins plotted. Simulation lines are monochromatic, the Huygens landing site data are purple. Bins with direct Huygens landing site observations have dots plotted over the lines, with larger dots indicating more observations. Bins on the Huygens landing site lines without dots are interpolated values. Note that the vertical axis scale is different for each wavelength.

could for Figures 6-8, and even the azimuth skewer only covers about a third of the available values. Cassini's observations geometries for the Huygens landing site do not probe the higher incidence and emission angles, and the extremes aren't even approached. Thus, we move to a much larger data set: the dunes.
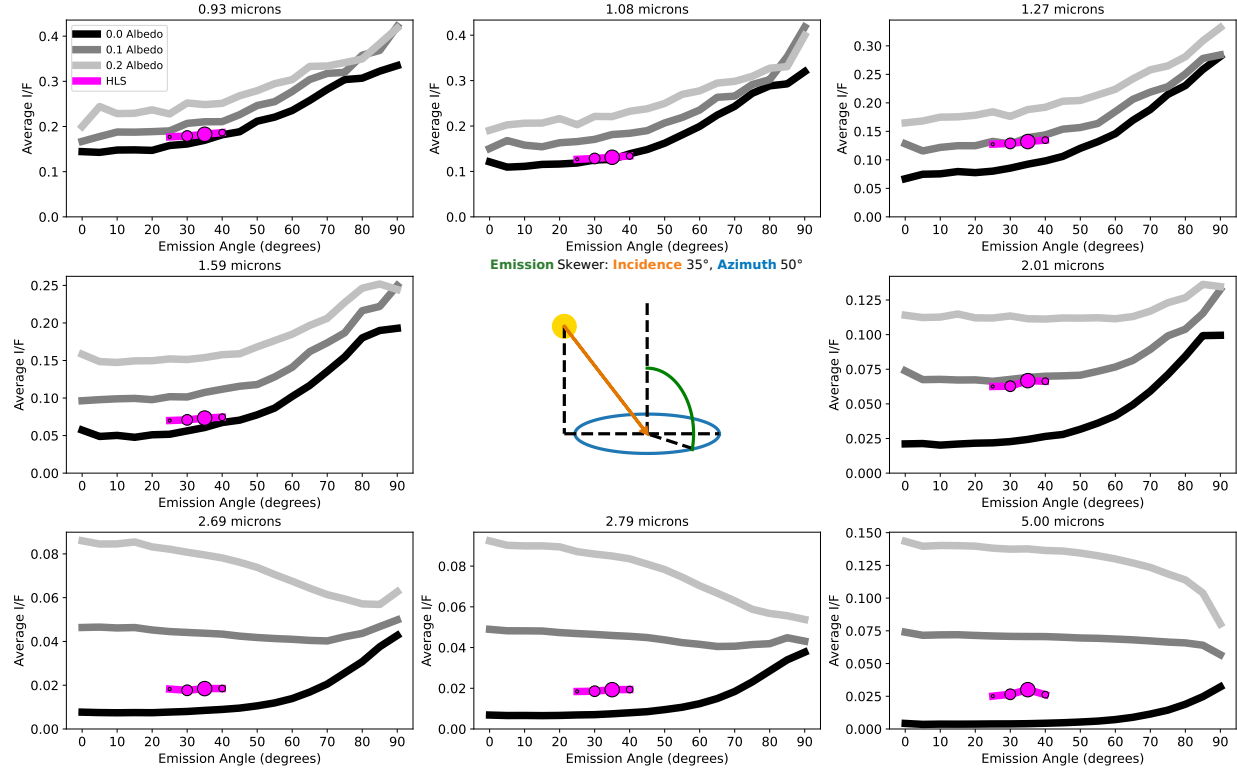
5.2. *Equatorial Dunes*

Similarly to the Huygens landing site data, we plot a variety of select one-dimensional skewers for the dunes. We plot more than three as the dunes data cover a far wider range of viewing geometries, focusing on incidence skewers for Figures 9-11.
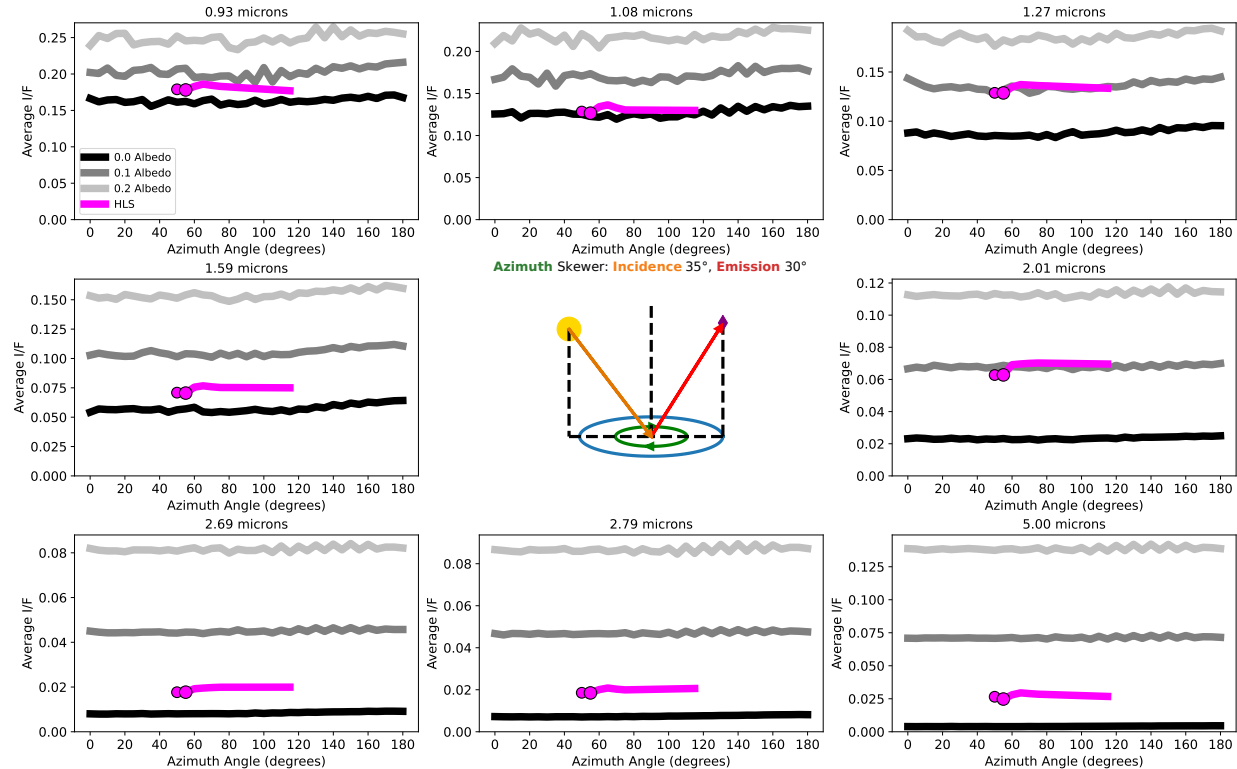
We find that most incidence skewers share a similar shape, visible in both Figure 9 and Figure 10. Higher incidence angles have lower I/F across the board, the exception being skewers with high emission and low azimuth where haze forward scattering becomes important. The dunes data match the shape of the simulations very well in these views, though incidences higher than $80°$ should be taken with a grain of salt, as Cassini aquired few observations near to and beyond the terminator. That said, the few points that do exist here match the simulated results well.

Curiously, the 2 μm restricted BDRF has a very noticeable shift in retrieved albedo for the dunes between the incidence skewers in Figure 9 and Figure 10, going from hugging the 0.1 albedo simulation to hanging somewhere around 0.05 albedo. 1.27 μm may do this as well, though it is harder to tell because the gap between 0.1 and 0.0 albedo simulations is smaller in that window and the data are less consistent. Comparing several incidence skewers reveals that this effect is emission-dependent, with larger emission values returning higher albedos. We will return to this effect when examining the emission skewers, as the effect is far more noticeable there.
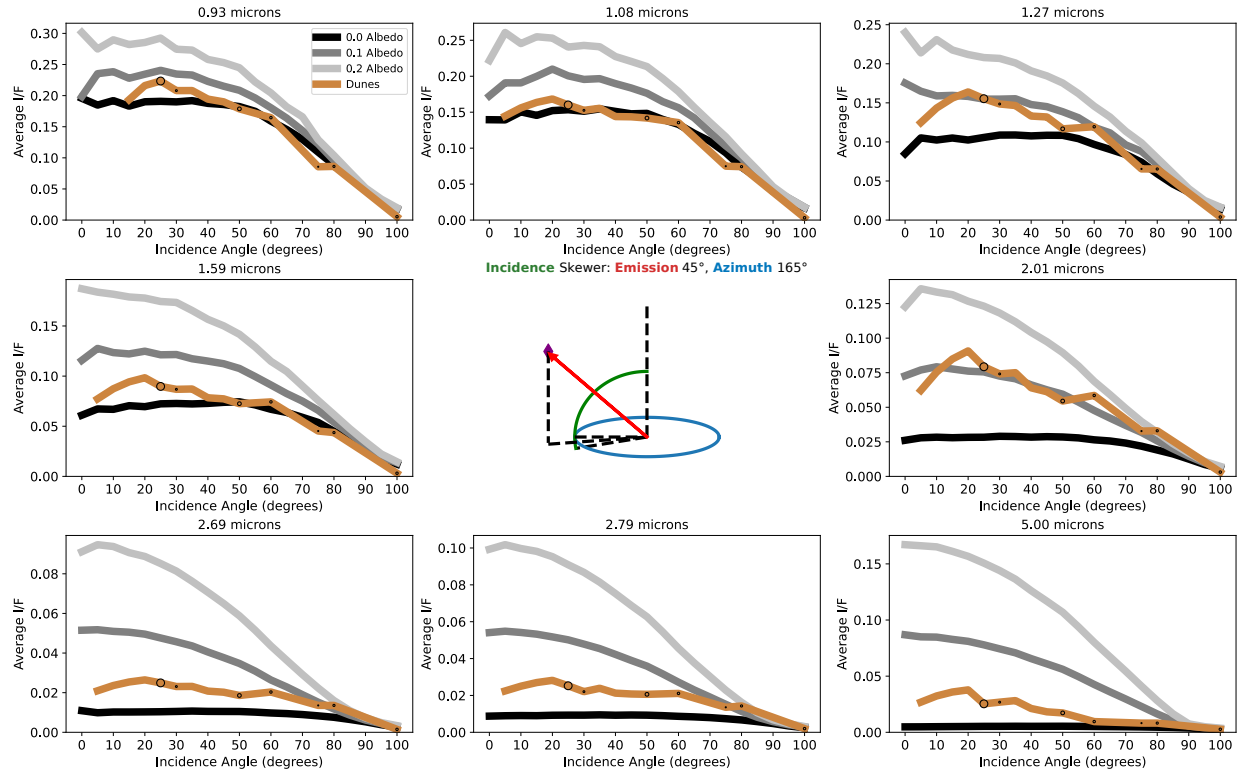
Most incidence skewers not shown look like Figure 9 and Figure 10 in the restricted BDRFs, except for those where no observations match the indicated geometry. The dunes data usually match the simulations in shape rather well, indicating Lambertian behavior when varying incidence. However, there are exceptions that happen at high emission and high azimuth, as exemplified by Figure 11. Here, the 2.01, 2.69, and 2.79 μm windows do not have slopes that match the simulations. Unfortunately, there are few points in this view, so this anomaly is hard to draw conclusions from. We will
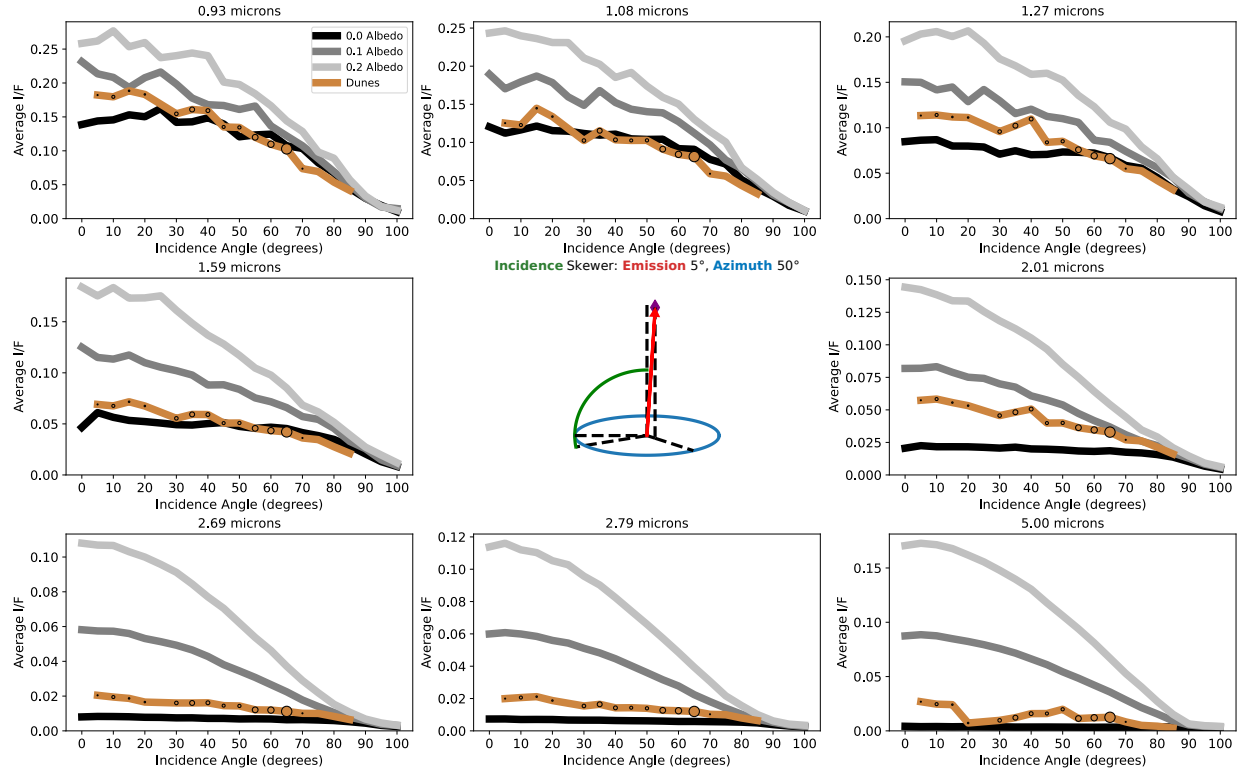
Figure 7. Same as Figure 6 but is instead a skewer through the emission angle, with incidence and azimuth held fixed.
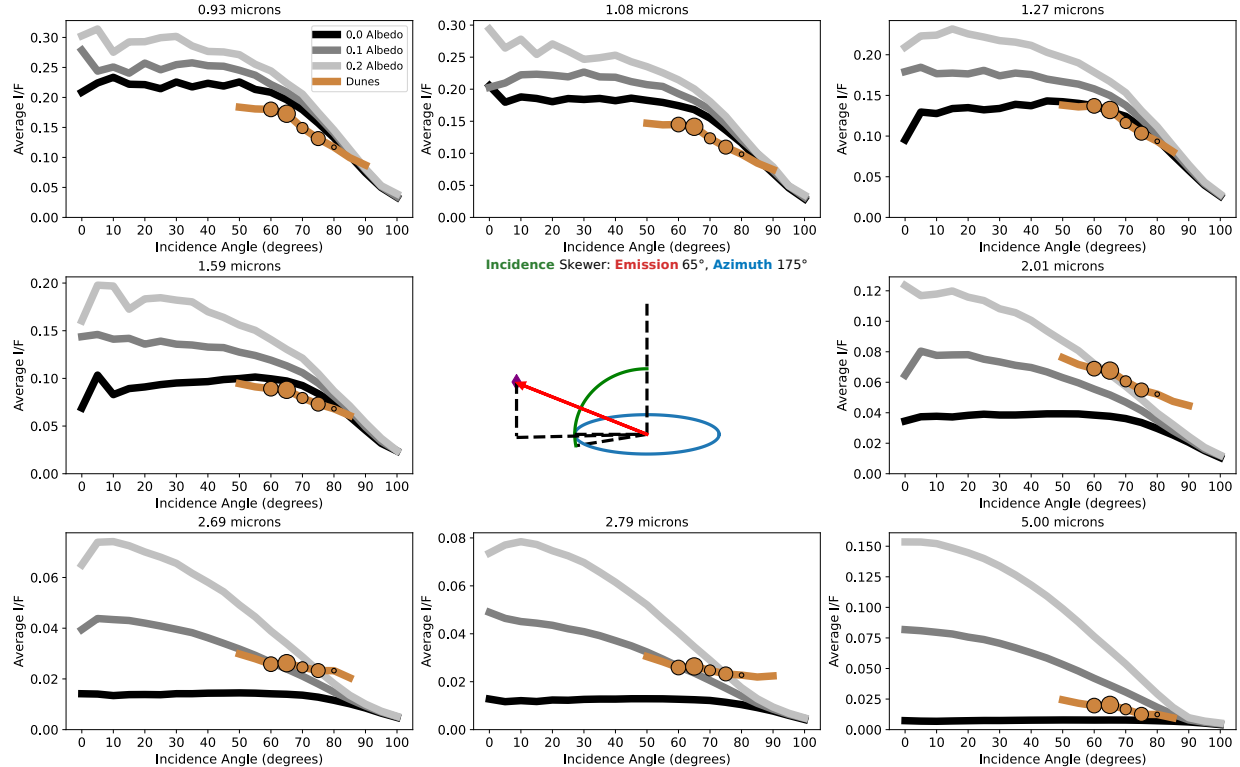

Figure 8. Same as Figure 6 but is instead a skewer through the azimuth angle, with incidence and emission held fixed.

Figure 9. Incidence angle skewer for Titan's dunes: incidence angle versus average I/F comparing restricted BDRFs with dunes data with fixed emission and azimuth angles. Showcases all eight wavelengths arranged from shortest to longest, with the central area occupied by a geometry diagram to illustrate the exact situation plotted. Simulation lines are monochromatic, dunes data are brown. Places with direct dunes observations have dots plotted over the lines, larger dots meaning more observations. Places on the dunes lines without dots are interpolated values. Note that the vertical axis scales with the data; not all wavelengths produce the same average I/F scale.

Figure 10. Same as Figure 9 but at different fixed emission and azimuth angles.

Figure 11. Same as Figure 9 but at different fixed emission and azimuth angles.

return to this slope anomaly when examining the emission skewers, as they shed some light on it.

Figure 11 also makes clear a physical impossibility that sometimes crops up in incidence slices: while the 0.93 and 1.08 μm windows have dune data shapes that match the simulations', the retrieved albedo is below 0.0, an impossibility. This may be because SRTC++ does not account for Rayleigh scattering, which is most relevant at short wavelengths (Essayeh et al. 2023). Intuitively, one would expect adding Rayleigh scattering to make the simulation brighter, not dimmer, but subtle effects could be at play–to fully answer this question, we would have to implement Rayleigh scattering, which is on the list for future improvements to SRTC++.

Emission skewers (where incidence and azimuth are held constant) for the restricted BDRFs generally show gradual increases in brightness with larger emission, though 5 μm is a notable exception, showing both limb darkening and limb brightening at different surface albedos. Selected views can be seen in Figures 12-14. Figure 12 and Figure 13 clearly show that for low emission angles, up to around 40°, the data match the simulations pretty well. However, at higher emission angles, this fails: Figure 12 shows the 0.93 - 1.59 μm windows dipping below the 0.0 albedo simulation at higher emission, while 2.01 - 2.79 μm do the opposite and sharply tick above the simulations. The dramatic brightening of 2.01 - 2.79 μm at high emission is just as strong, if not stronger, in Figure 13, showing azimuthal independence of this effect. However, the 0.93 - 1.59 μm dimming below the 0.0 albedo simulation is not as strong, and doesn't clearly exist at the 1.27 μm and 1.59 μm windows. The dimming effect in the 0.93 - 1.59 μm windows vanishes entirely in Figure 14, while the brightening for 2.01 - 2.79 μm effect remains. (Notably, Figure 14 has few data points at high emission, but the fact that it follows the pattern laid out in other nearby skewers gives us confidence that its behavior is not just an interpolation artifact). These brightening and darkening effects explain the inconsistent retrieved albedo and values below 0.0 albedo noted in the incidence skewers; these deviations are emission dependent. Furthermore, the fact that brightening only occurs in 2.01 - 2.79 μm windows and that these are the only windows seen not matching the simulations in Figure 11 lends further credence that Figure 11's deviations are not just a bad series of observations.
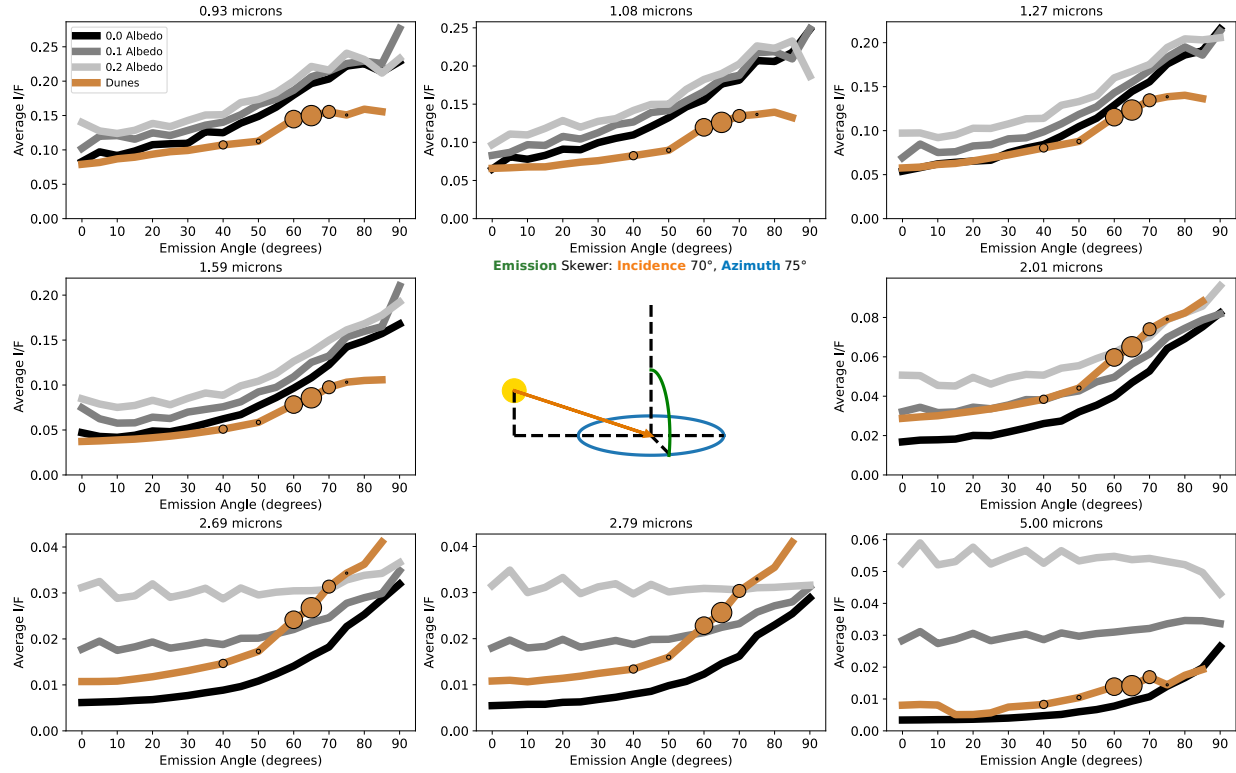
So, how can we explain the variablity in retreived abledo across the various emission angles? There are two primary explanations. First, the model does not accurately account for some atmospheric effect at high emission. While we mentioned Rayleigh Scattering earlier, that will only have an important effect on short wavelengths (Es-sayeh et al. 2023). We suspect that the haze model is where the problem lies, as at higher emission angles, light escaping from the surface has to pass through a lot of atmospheric haze; if our model thinks the haze is thicker than it is in reality, more light will be let through unimpeded as emission rises. It is true that higher incidence angles (up to a point) will also result in a longer path through the haze; however, this will be counteracted by the fact that any spot on the surface of Titan is going to be diffusely illuminated due to light scattering from other directions. Whether the source of the discrepancies lies in the atmospheric model or the way the code treats it is unknown at this juncture.
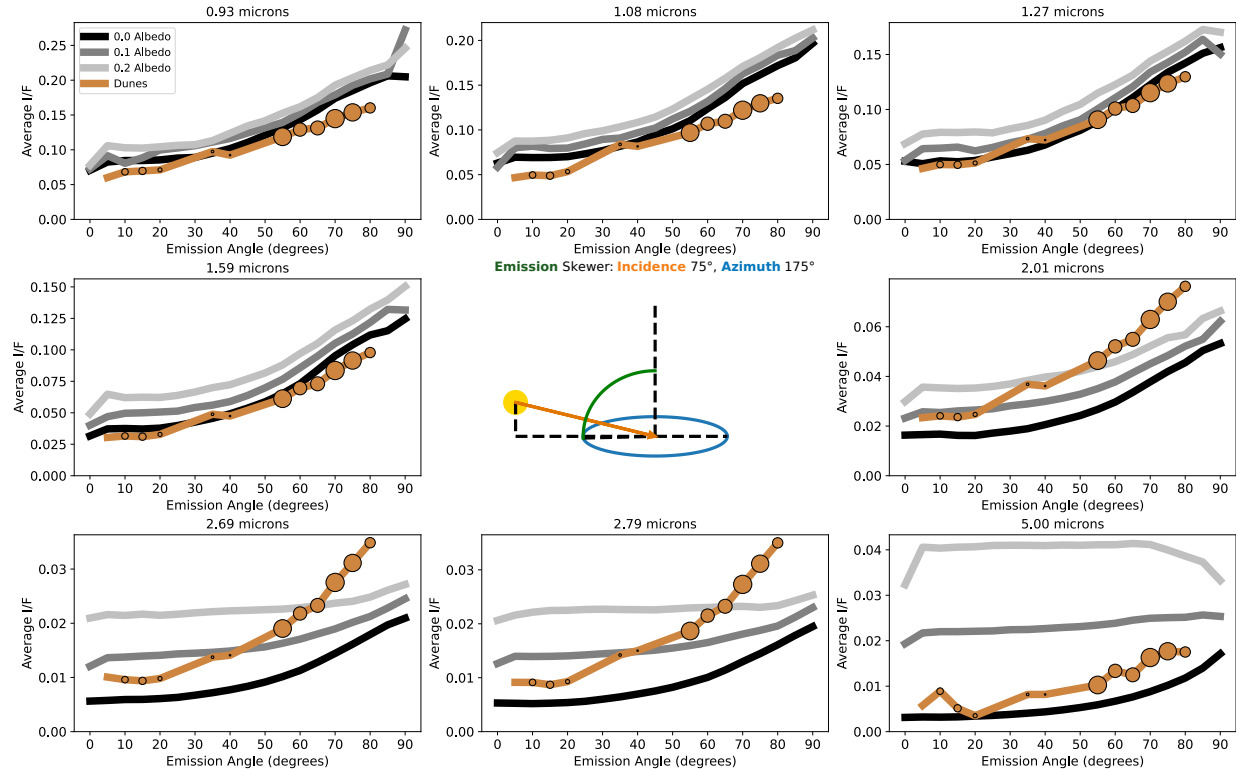
The second explanation is that we're seeing a true non-Lambertian effect from the surface. However, this seems unlikely, as the brightening effect appears azimuthally agnostic: no matter what azimuth we point at, the emission effect exists where we have enough data to see it, and a forward-scattering or backscattering effect would be particularly focused at 0° or 180°, not present everywhere. Topogrpahy oriented explanations also seem unlikely, since the effect begins around 40° and only extreme emission angles should be greatly influenced by topography. Not to mention the fact that Titan is rather smooth, topographically speaking, with only a couple km elevation variation on the surface (Corlies et al. 2017). That said, if we eventually rule out a deficiency in the simulation, we would be forced to consider a surface effect, which would be investigated in future work by testing out various non-Lambertian BRDFs for the surface in the SRTC++ simulations and observing if any of them led to azimuthally agnostic effects.

Despite this clear deviation at high emission, overall, simulation and data still match remarkably well. Nowhere is this easier shown than the azimuth skewers, which, unlike the incidence and emission skewers, regularly have data in large numbers and data points covering the entire range. In most situations, the result is flat, such as in Figure 15 and Figure 16.
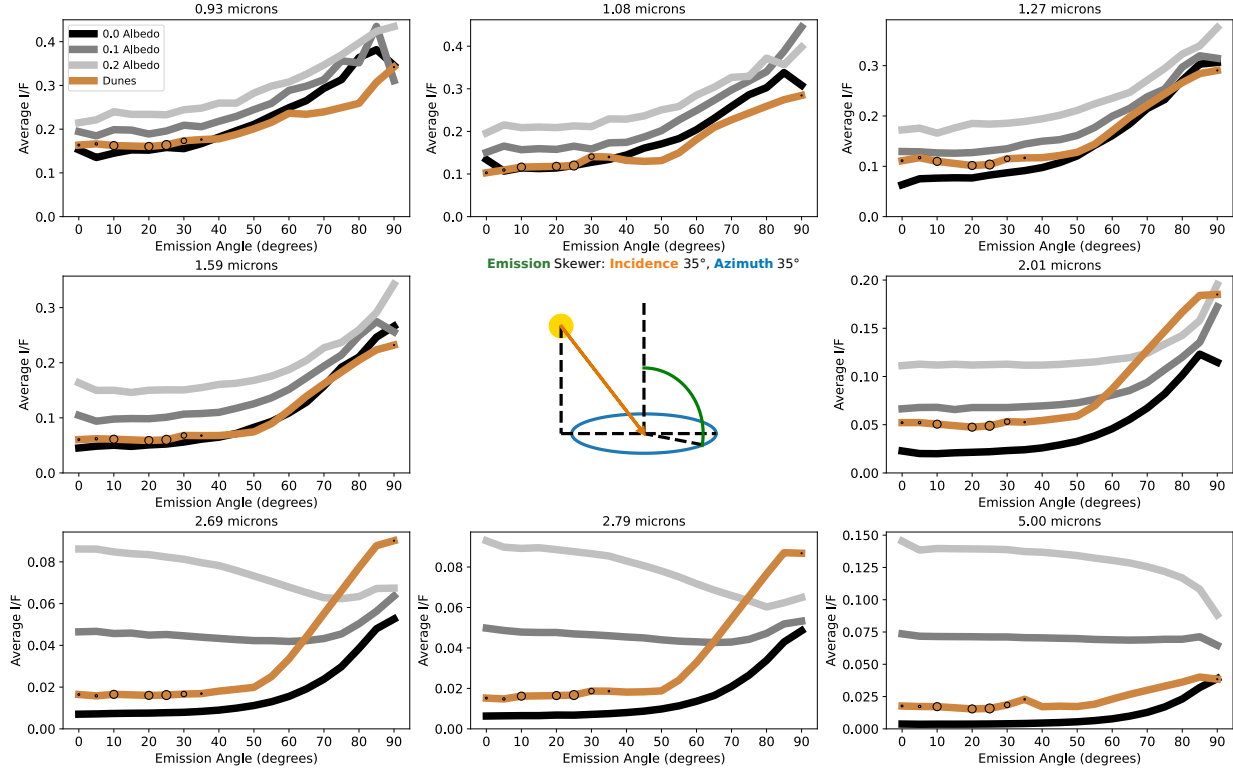
Most azimuth views are completely flat in both simulation and real data. The exception to the flatness is when both incidence and emission are high at the same time, at which point the simulations predict forward scattering, as can be seen in Figure 17. This low azimuthal brightness represents atmospheric forward scattering. Unfortunately, we have very few observations in this region of the restricted BDRF, and the interpolation is rather suspect as there aren't other regions with similar behavior as was the case with the emission skewers. Figure 17's interpolation still shows an uptick at low azimuth despite the lack of data, which at least suggests that the behavior is plausibly accurate. One saving grace is that at such angles, the effects of the atmosphere take over and almost drown out the surface effects, so the dunes themselves are unlikely to have much effect on real observations in the first place. Note that in Figure 17 the different albedo values are all very closely clustered together and nearly identical in shape, corroborating this thought. Even though the 5 μm
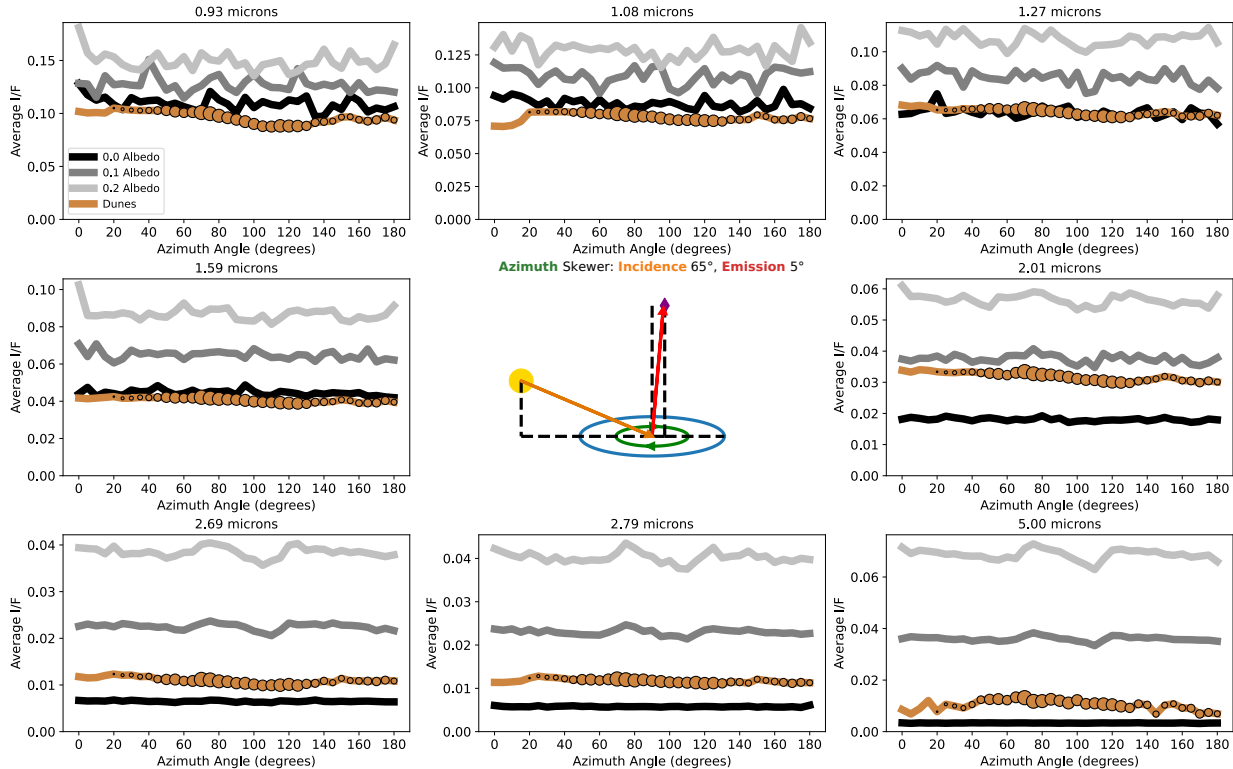
Figure 12. Same as Figure 10 but is instead a skewer through the emission angle, with incidence and azimuth held fixed.
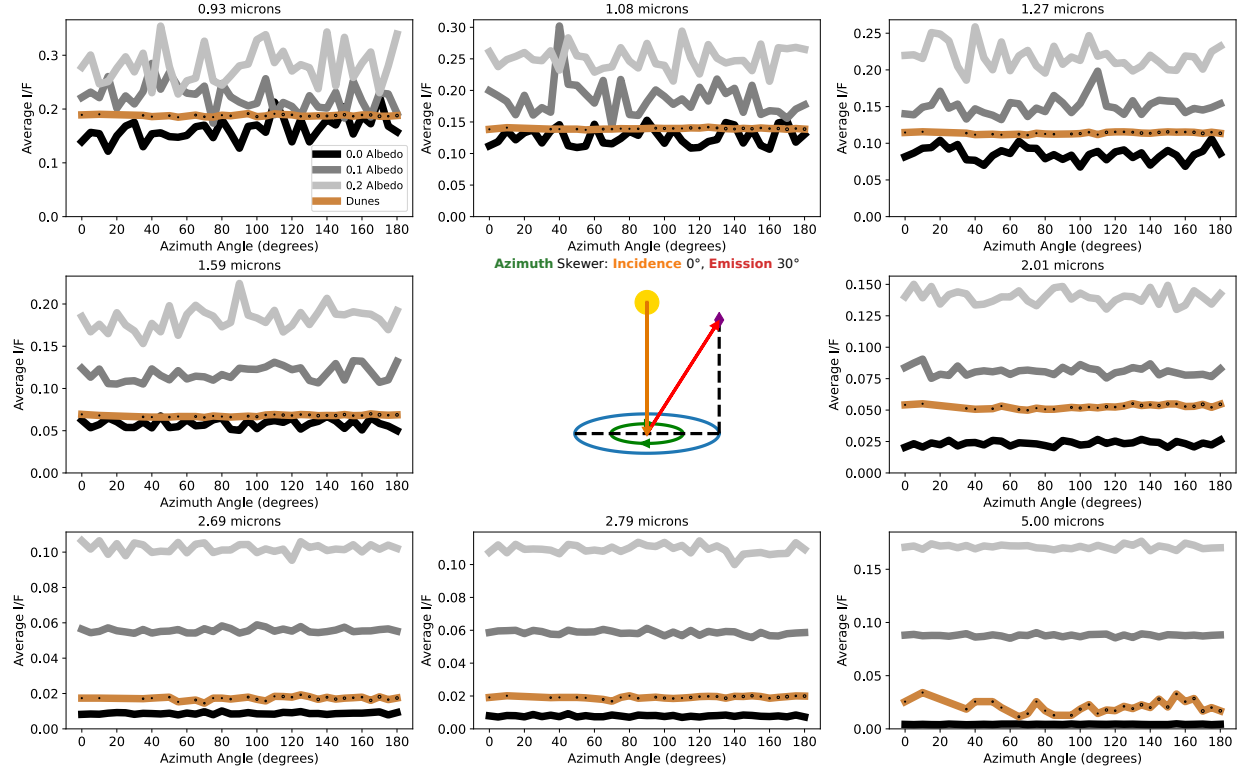

**Figure 13.** Same as Figure 12 but at different fixed incidence and azimuth angles.
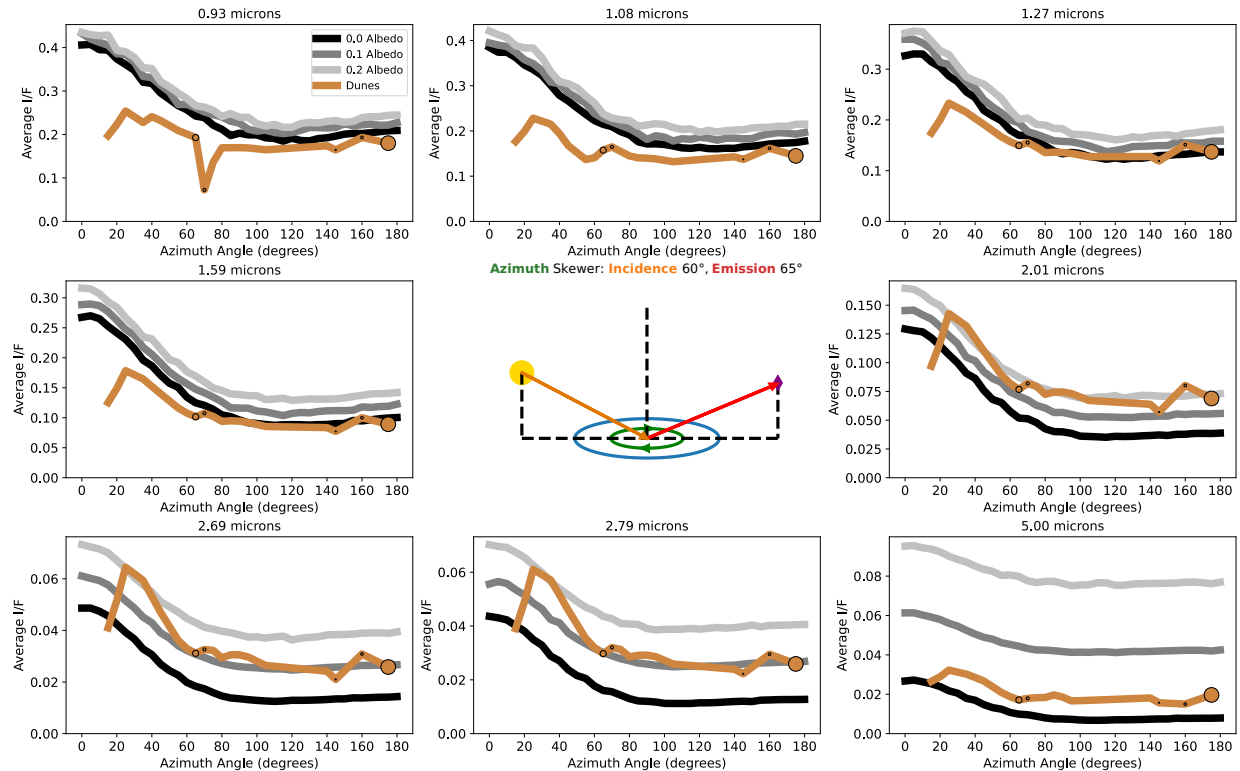
**Figure 14.** Same as Figure 12 but at different fixed incidence and azimuth angles.

Figure 15. Same as Figure 10 but is instead a skewer through the azimuth angle, with incidence and emission held fixed.

Figure 16. Same as 15 but at different fixed incidence and emission angles.

Figure 17. Same as 15 but at different fixed incidence and emission angles.

window appears to have a large spread between its simulated curves, this seeming variability is merely due to the fact that all the simulations report very dim I/F values, differing only by 0.05 overall.

In the end, where do these simulation and observation comparisons leave us? With the shapes of the dunes data matching the restricted BDRFs so closely in incidence and azimuth, it seems reasonable to conclude that the dunes act substantially as a Lambertian surface. The primary evidence for non-Lambertian behavior comes from the inconsistent albedo retrieval at variable emission, which does not appear to have an azimuthal dependence and is likely an atmospheric effect not accounted for in the simulation, rather than a true non-Lambertian effect. The other minor deviation in Figure 11's slope for 2.01 and 2.79 μm correlates directly with the windows brightening in emission skewers, tying the two effects together, lowering our expectations of observing a true non-Lambertian effect even further.

However, we recognize that our method of binning spectels together and averaging them all makes us significantly less sensitive to dramatic changes over tiny angular extents, such as the sharp central peak often seen in the opposition effect, sometimes less than one degree away from opposition (Kulyk 2008; Schaefer et al. 2008). It is worthwhile to perform a more focused check for such an effect.

6. OPPOSITION EFFECT SEARCH

We actively looked for opposition effects in the dune data discussed above, examining every skewer we had. The opposition effect would occur at places where incidence and emission were close to each other, and azimuth was at or near 180°. We unfortunately had very few data exactly at these points, but if the opposition effect were somewhat broad on Titan, we would have expected to still see some "humps" in the data that would not have been replicated in the simulations. We did not find any such humps. Pseudospecular forward scattering is not a component of the opposition effect, though it would be similarly placed in the restricted BDRFs, just at 0° azimuth instead. We also do not observe it in our skewers.

However, we would not have noticed an extremely sharp opposition effect, as it could conceivably only matter at angles extremely close to direct opposition; that is, near 0° incidence, 0° emission, 180° azimuth. Our dunes data only have a handful of points around this region, and it is at the very border of the restricted BDRFs, so looking at skewers is rather unhelpful.
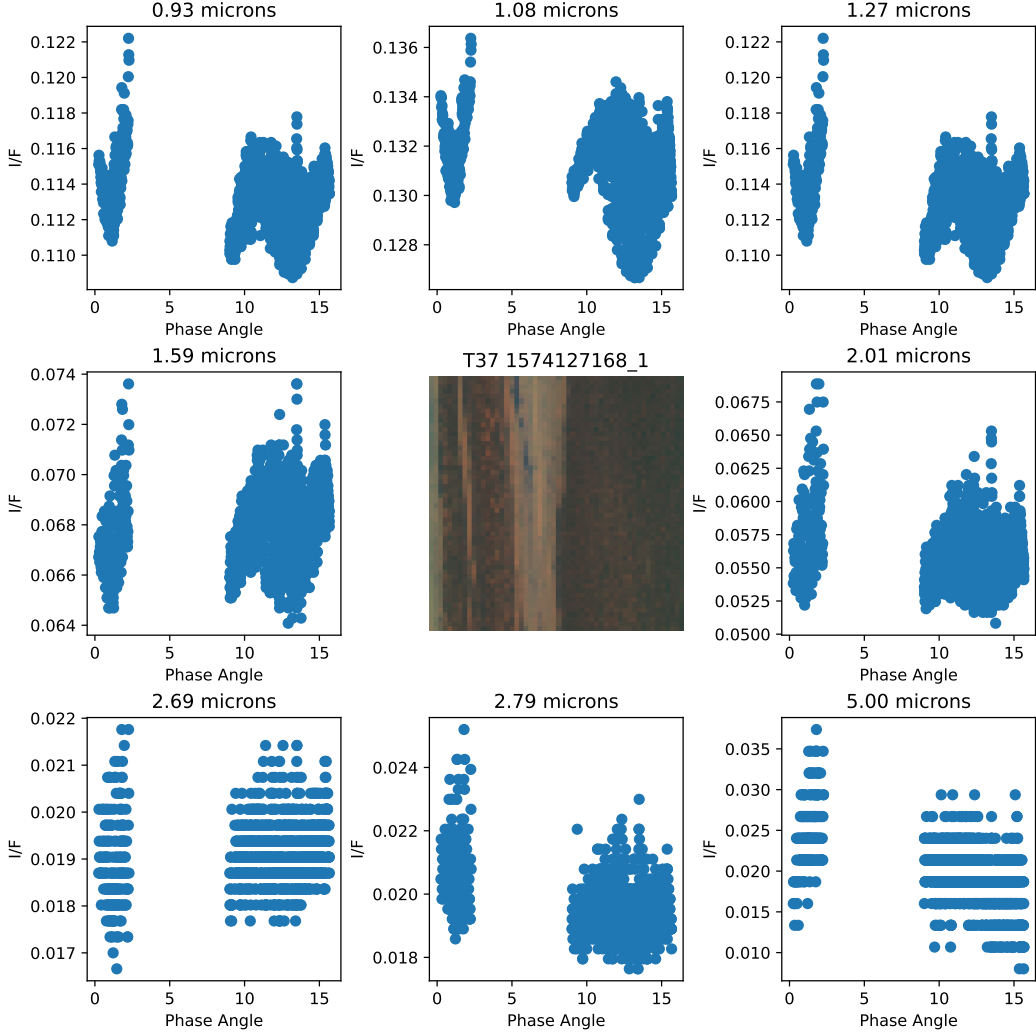
Instead, we went back to the original VIMS cube files and looked for ones of the dunes that had viewing geometries within 1° of opposition. Precisely one cube in our data set that met this criterion: cube 1574127168_1 from flyby T37. We then took the data from this cube and plotted its I/F versus the phase angle, which is a measure of how close each pixel was to opposition. The result is Figure 18.

While there does appear to be a spike in Figure 18, it happens at around 3° and vanishes as we approach actual opposition. We can identify this feature with a slightly brighter section of the dunes in the lower left of the cube, near the central non-dune strip. We must consider the possibility that this could be a pointing error; retrieved coordinates on Titan's surface are known to be off by a degree at times (Barnes et al. 2008). Due to the stretching of the cube, the brighter section is within one geographical degree of the pixels labeled closest to opposition. We examined other VIMS views of the nearby geography from different flybys in Figure 19 and found that the dunes consistently get slightly brighter in that direction (north), regardless of viewing geometry, so the spike is most likely a persistent feature and not a very narrow opposition effect.

Curiously, there appears to be a slight uptick in brightness toward direct opposition in the three shortest wavelength windows, though this is within the average intensity of other dunes pixels, so it does not constitute any opposition effect. Furthermore, we must contend with the fact that the opposition effect is all but removed by diffuse lighting and indirect viewing angles from scattering (Schröder & Keller 2008), which certainly occurs at the lower wavelength windows, making it so we would not expect to see any kind of signal here. That said, this is not true at other windows. 5.00 μm in particular sees significant unimpeded sunlight even when it is near sunset (Barnes et al. 2018). If there were an opposition effect being hidden by the atmosphere, then we would expect to see it in 5.00 μm, but we do not. Figure 18's 5.00 μm window has some of the least evidence of a spike out of all windows.

With the spike at 3° explained, we find that the increase in brightness with proximity to opposition appears vaguely linear, which is expected (Kulyk 2008), though in a few windows the spread of intensities is such that no brightening trend can be discerned. Here, we end our search, concluding that we observe no opposition effect in the dunes to the limits of VIMS' cabability to measure. The closest point to true opposition is reported as 0.25° degrees away; assuming this is correct, even it does not entirely rule out a narrow and sharp opposition effect, as these can be confined to within 0.1° (Kulyk 2008; Schaefer et al. 2008). The Solar disc's footprint on Titan is around 0.05deg (Barnes et al. 2011), further implying it would not be detectable. Huygens observed the opposition effect spike to begin around 0.2° (Karkoschka et al. 2012), and the observation was made with Huygens' own illumination, not the sun's. The viewing gometry to definitively confirm or deny the opposition effect simply does not exist in the Cassini data for the dunes; we can only say that if the dunes

Figure 18. Cube 1574127168_1 from flyby T37 with dunes spectels separated out and plotted by opposition proximity and I/F in all eight windows. The cube itself is plotted in the center with a color scheme of red 5.00 μm, green 2.01 μm, and blue 1.27 μm. Note that the image is significantly stretched; the actual surface of Titan covered by this image is significant and greatly extended in the horizontal direction. The gap in the middle of the points exists due to those pixels not being dune pixels. Note that most of the points follow a generally linear trend, with the exception of a single spike at around 3° from opposition. We can visually see some somewhat brighter dunes pixels in the central image in the upper right, which no doubt cause this spike. The physical location of the pixels closest to true opposition is in the upper left region.

have an opposition effect, it is a narrow one with little-to-no broad component.
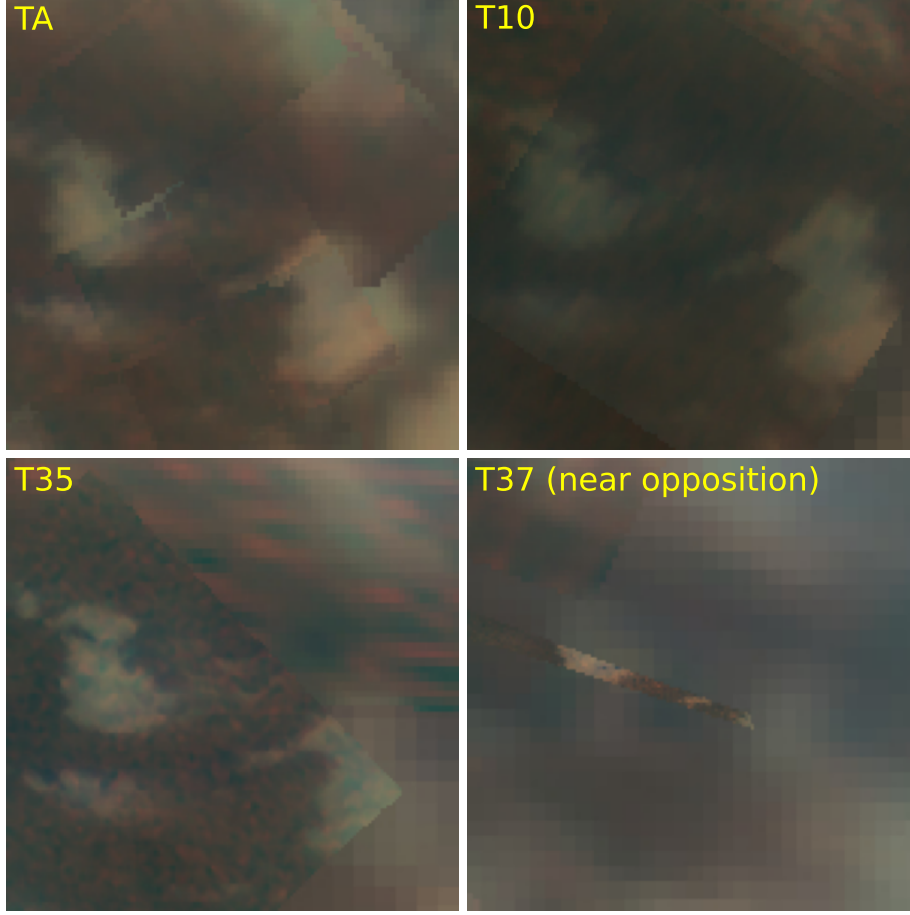
7. SUMMARY AND CONCLUSION

There were two primary purposes to this paper: to validate the SRTC++ simulation against real data, and to identify how Lambertian Titan's dunes were.

On the validation front, SRTC++ in general calculated restricted BDRF trends that matched the real data, but clearly didn't always produce the correct albedo, as evidenced by situations where the recovered albedo is below 0.0, an impossibility. As these moments primarily occur at short wavelengths, the impossible albedos could be the influence of Rayleigh Scattering. Alternatively, or perhaps additionally, its source could be a fault in the characterization of atmo-

spheric haze–the deviations along emission skewers imply there's certainly something missing there.

Despite these caveats, SRTC++ still produces smooth lines parallel to the real data in most incidence and azimuth skewers, only with inconsistent albedo results. As such, the simulations are still useful for characterizing Titan's surface, particulary looking for clear deviations from the Lambertian assumption. It is telling, then, that we found almost none. There is no evidence of an opposition effect and no evidence for a forward scattering component to the surface BDRF. The only potential deviation is the dimming and brightening some windows exhibit at high emission angles–but as this effect is azimuthally agnostic, we attribute its deviation to atmospheric mischaracterization.

Figure 19. Cylindrical projections of Titan near the opposition observation in flybys TA-, T10, and T35, with the opposition flyby itself (T37) there for comparison. The cylindrical projections are made in a manner similar to Barnes et al. (2009), but from singular flybys only. While in T37 itself the observations are not of high enough quality to see, the others show that the dunes get slightly brighter to the north, consistent with a shift in dune properties, not an opposition effect.

Our ultimate conclusion is that Titan's dunes are Lambertian surfaces, or very close to it. This result is not unexpected, for Earth's sand is also generally Lambertian (Hapke & van Hoen 1963), though Earth's sand exhibits an opposition effect within two degrees of zero phase angle (Wise & Mars 2022), which would have been detectable were this the case on Titan. However, it is thought that the width of an opposition effect narrows the further an object is from the sun (Karkoschka et al. 2012) due to the smaller angular diameter of the solar disk, so we cannot say that we should have seen an opposition effect on the dunes. Furthermore, Earth's sand and Titan's dunes are characteristically different, as most of Earth's deserts are quite bright, while Titan's dunes are the darkest solid terrain on its surface.

Future work would include improving SRTC++ to simulate the atmosphere properly at high emission–or, if that were to prove impossible, investigating what other effects might cause the inaccuracies at high emission. If we cannot track down a specific issue with SRTC++ through this, we will investigate unusual surface BRDFs and see if any of them can produce an azimuthally agnostic effect when seen through the atmosphere. This work could also be turned to the specular lakes at Titan's north pole; while the atmosphere is not as well characterized there, we can use the relatively simple lake phase functions to probe where specifically it's poorly characterized. Other terrain types on Titan could also be examined–it would just require a manual rather than automated approach, as the other terrains are not as distinct as the dunes. Preliminary investigations on this front have been performed, but none of the other terrains (including equatorial bright) had results as reugular and as expansive as the dunes.

REFERENCES

705 Barnes, J. W., MacKenzie, S. M., Lorenz, R. D., & Turtle, E. P.
706 2018, The Astronomical Journal, 156, 247,
707 doi: 10.3847/1538-3881/aae519

708 Barnes, J. W., Brown, R. H., Turtle, E. P., et al. 2005, Science, 310,
709 92, doi: 10.1126/science.1117075

710 Barnes, J. W., Brown, R. H., Soderblom, L., et al. 2007, Icarus,
711 186, 242, doi: 10.1016/j.icarus.2006.08.0219

712 —. 2008, Icarus, 195, 400, doi: 10.1016/j.icarus.2007.12.006

713 Barnes, J. W., Soderblom, J. M., Brown, R. H., et al. 2009,
714 Planetary and Space Science, 57, 1950–1962,
715 doi: 10.1016/j.pss.2009.04.013

716 —. 2011, Icarus, 211, 722–731, doi: 10.1016/j.icarus.2010.09.022

717 Bonnefoy, L. E., Hayes, A. G., Hayne, P. O., et al. 2016, Icarus,
718 270, 222–237, doi: 10.1016/j.icarus.2015.09.014

719 Brossier, J. F., Rodriguez, S., Cornet, T., et al. 2018, Journal of
720 Geophysical Research: Planets, 123, 1089–1112,
721 doi: 10.1029/2017je005399

722 Buratti, B., Sotin, C., Brown, R., et al. 2006, Planetary and Space
723 Science, 54, 1498, doi: 10.1016/j.pss.2006.06.015

724 Cooper, C. A., Robinson, T. D., Barnes, J. W., Mayorga, L. C., &
725 Robinthal, L. 2025, Extreme Forward Scattering Observed in
726 Disk-Averaged Near-Infrared Phase Curves of Titan, arXiv,
727 doi: 10.48550/ARXIV.2507.00924

728 Corlies, P., Hayes, A. G., Birch, S. P. D., et al. 2017, Geophysical
729 Research Letters, 44, doi: 10.1002/2017gl075518

730 Corlies, P., McDonald, G. D., Hayes, A. G., et al. 2021, Icarus,
731 357, 114228, doi: 10.1016/j.icarus.2020.114228

732 Déau, E., Dones, L., Rodriguez, S., Charnoz, S., & Brahic, A.
733 2009, Planetary and Space Science, 57, 1282,
734 doi: 10.1016/j.pss.2009.05.005

735 Es-sayeh, M., Rodriguez, S., Coutelier, M., et al. 2023, The
736 Planetary Science Journal, 4, 44, doi: 10.3847/PSJ/acbd37

737 García Muñoz, A., Lavvas, P., & West, R. A. 2017, Nature
738 Astronomy, 1, doi: 10.1038/s41550-017-0114

739 Griffith, C. A., Doose, L., Tomasko, M. G., Penteado, P. F., & See,
740 C. 2012, Icarus, 218, 975, doi: 10.1016/j.icarus.2011.11.034

741 Hapke, B., & van Hoen, H. 1963, Journal of Geophysical
742 Research, 68, 4545–4570, doi: 10.1029/jz068i015p04545

743 Karkoschka, E., Schröder, S. E., Tomasko, M. G., & Keller, H. U.
744 2012, Planetary and Space Science, 60, 342–355,
745 doi: 10.1016/j.pss.2011.10.014

746 Kazeminejad, B., Atkinson, D. H., & Lebreton, J.-P. 2011, The
747 Astrophysical Journal Letters, 47, 1622–1632,
748 doi: 10.1016/j.asr.2011.01.019

749 Keller, H., Grieger, B., Küppers, M., et al. 2008, Planetary and
750 Space Science, 56, 728–752, doi: 10.1016/j.pss.2007.11.020

751 Kulyk, I. 2008, Planetary and Space Science, 56, 386–397,
752 doi: 10.1016/j.pss.2007.11.011

753 Le Mouélic, S., Cornet, T., Rodriguez, S., et al. 2012, Planetary
754 and Space Science, 73, 178–190, doi: 10.1016/j.pss.2012.09.008

755 —. 2019, Icarus, 319, 121–132, doi: 10.1016/j.icarus.2018.09.017

756 Lopes, R. M. C., Malaska, M. J., Schoenfeld, A. M., et al. 2020,
757 Nature Astronomy, 4, 228, doi: 10.1038/s41550-019-0917-6

758 Lynch, D. K., & Livingston, W. 2004, Color and light in nature
759 (Cambridge Univ. Press)

760 Neish, C. D., Lorenz, R. D., Kirk, R. L., & Wye, L. C. 2010,
761 Icarus, 208, 385–394, doi: 10.1016/j.icarus.2010.01.023

762 Pont, S. C., & Koenderink, J. J. 2007, Perception amp;
763 Psychophysics, 69, 459–468, doi: 10.3758/bf03193766

764 Rannou, P., Coutelier, M., Rivière, E., et al. 2021, The
765 Astrophysical Journal, 922, 239,
766 doi: 10.3847/1538-4357/ac2904

767 Rodriguez, S., Le Mouélic, S., Sotin, C., et al. 2006, Planetary and
768 Space Science, 54, 1510–1523, doi: 10.1016/j.pss.2006.06.016

769 Rodriguez, S., Le Mouélic, S., Barnes, J. W., et al. 2018, Nature
770 Geoscience, 11, 727–732, doi: 10.1038/s41561-018-0233-2

771 Schaefer, B. E., Rabinowitz, D. L., & Tourtellotte, S. W. 2008, The
772 Astronomical Journal, 137, 129–144,
773 doi: 10.1088/0004-6256/137/1/129

774 Schröder, S., & Keller, H. 2008, Planetary and Space Science, 56,
775 753–769, doi: 10.1016/j.pss.2007.10.011

776 —. 2009, Planetary and Space Science, 57, 1963–1974,
777 doi: 10.1016/j.pss.2009.03.012

Seal, D., & Bittner, M. 2017, in 2017 IEEE Aerospace Conference (IEEE), 1–12, doi: 10.1109/aero.2017.7943848

Seignovert, B., Mouélic, S. L., Heslar, M., et al. 2023, PyVIMS, Zenodo, doi: 10.5281/ZENODO.4708004

Soderblom, L. A., Kirk, R. L., Lunine, J. I., et al. 2007, Planetary and Space Science, 55, 2025, doi: 10.1016/j.pss.2007.04.014

Soderblom, L. A., Brown, R. H., Soderblom, J. M., et al. 2009, Icarus, 204, 610, doi: 10.1016/j.icarus.2009.07.033

Solomonidou, A., Malaska, M., Lopes, R., et al. 2024, Icarus, 421, 116215, doi: 10.1016/j.icarus.2024.116215

Sullivan, C. B., & Kaszynski, A. A. 2019, Journal of Open Source Software, 4, 1450, doi: 10.21105/joss.01450

Tomasko, M. G., Doose, L., Engel, S., et al. 2008, Planetary and Space Science, 56, 669, doi: 10.1016/j.pss.2007.11.019

Vinatier, S., Bezard, B., Fouchet, T., et al. 2007, Icarus, 188, 120–138, doi: 10.1016/j.icarus.2006.10.031

Wise, J. E., & Mars, J. C. 2022, Remote Sensing, 14, 5020, doi: 10.3390/rs14195020

Wye, L. C. 2011, Radar scattering from Titan and Saturn's icy satellites using the Cassini spacecraft (stanford university)

Xu, F., West, R. A., & Davis, A. B. 2013, Journal of Quantitative Spectroscopy and Radiative Transfer, 117, 59, doi: 10.1016/j.jqsrt.2012.10.013